Low-voltage anodizing of copper in sodium bicarbonate solutions

Brudzisz, Anna; Giziński, Damian; Liszewska, Malwina; Wierzbicka, Ewa; Tiringer, Urša; Taha, Safeya A.; Zając, Marcin; Orzechowska, Sylwia; Jankiewicz, Bartłomiej; Taheri, Peyman

DOI
10.1016/j.electacta.2023.141918

Publication date
2023

Document Version
Final published version

Published in
Electrochimica Acta

Electrochimica Acta 443 (2023) 141918

Contents lists available at ScienceDirect

Electrochimica Acta

journal homepage: www.journals.elsevier.com/electrochimica-acta

Low-voltage anodizing of copper in sodium bicarbonate solutions

Anna Brudzisz [a,*], Damian Giziński [a], Malwina Liszewska [b], Ewa Wierzbicka [a], Urša Tiringer [c], Safeya A. Taha [d], Marcin Zając [e], Sylwia Orzechowska [f], Bartłomiej Jankiewicz [b], Peyman Taheri [c], Wojciech J. Stępniowski [a]

[a] Institute of Materials Science and Engineering, Faculty of Advanced Technologies and Chemistry, Military University of Technology, 2 Kaliskiego Street, 00908 Warsaw, Poland
[b] Institute of Optoelectronics, Military University of Technology, 2 Kaliskiego Street, 00908 Warsaw, Poland
[c] Department Material Science and Engineering, Faculty of Mechanical, Maritime and Materials Engineering, Delft University of Technology, 2 Mekelweg, 2628 CD Delft, the Netherlands
[d] Department of Physics, Sphinx University, New Assiut City, Assiut, Egypt
[e] SOLARIS National Synchrotron Radiation Centre, Jagiellonian University, 98 Czerwone Maki Street, 30392 Krakow, Poland
[f] Department of Chemical Physics, Faculty of Chemistry, Jagiellonian University, Gronostajowa 2, 30387 Krakow, Poland

ARTICLE INFO

Keywords:
Copper
Electrooxidation
Malachite
Carbon dioxide reduction reaction
Anodic films

ABSTRACT

The low-voltage (< 5 V) anodization of copper in aqueous solutions of sodium bicarbonate was studied for the first time. As demonstrated, this method leads to the formation of microstructures on a copper surface, that are composed of malachite ($CuCO_3{\cdot}Cu(OH)_2$). Moreover, by tuning the operating conditions, i.e., applied cell voltage and electrolyte concentration, different surface morphologies can be grown. As shown by electron microscopy investigation, clusters of ribbons corrosion pits or nonuniformly located powdery precipitates are formed when the low anodizing voltage is applied. Anodization at 1.0 V in 0.4 M sodium bicarbonate solution led to the formation of a velvet-like, deep black anodic layer that covered the whole metal surface with ribbon-resembling structures. A thorough investigation of the obtained anodic layers with X-ray diffraction (XRD), X-ray adsorption (XAS), Raman, and X-ray Photoelectron Spectroscopy (XPS) uncovered the mixed crystalline-amorphous nature of the anodic copper species. Besides dominating the crystalline malachite phase, the amorphous cupric oxide was also identified. This composition offers promising features for catalytic applications, hence, low-voltage anodized copper was tested in an electrochemical CO_2 reduction reaction to explore one possible application of the presented material. The current density of 4.7 mA cm^{-2} was registered for the selected sample.

1. Introduction

Development of novel nano- and micro-structured materials, with a highly developed surface area, especially semiconductor metal oxides, is considered one of the most relevant matters within the field of materials science. This is due to their exceptional properties and applicability, especially in photocatalysis [1–3]. Notably, copper oxides, i.e., CuO and Cu_2O, with a relatively narrow bandgap of 1.6 to 2.0 eV, seem to be attractive materials for applications in catalyzing photoinduced processes [4,5].

Nanostructured copper oxides and hydroxide can be obtained by chemical [6,7], thermal [8,9], and electrochemical [4] methods. The most interesting aspect that has to be considered while discussing CuO_x synthesis, is the fact that there is a variety of morphologies and compositions that can be achieved by available methods. These features directly determine the practicality of a particular material application. Further development of well-known methods of synthesis should include economic considerations and eventual implementation in industrial-scale production. The most commonly used techniques, such as annealing, are already applied in large-scale production, however, the diversity of morphologies obtained with the method is strongly limited [9]. More recently, due to simplicity and low costs, electrochemical methods (i.e., electrooxidation and electroreduction) began to be re-explored for the formation of nanostructured Cu, Cu_2O, CuO, $Cu(OH)_2$, and other copper derivatives for more currently relevant applications [10–15]. Such materials have been successfully used in batteries, direct methanol fuel cells, oxygen evolution reaction, photocatalysis, and carbon dioxide reduction reaction (CO_2RR). Increasing interest in

* Corresponding author.
E-mail address: anna.brudzisz@wat.edu.pl (A. Brudzisz).

https://doi.org/10.1016/j.electacta.2023.141918
Received 8 November 2022; Received in revised form 23 December 2022; Accepted 17 January 2023
Available online 18 January 2023

the electrochemical formation of oxidized copper is related to unique features of as-prepared Cu-derived materials, such as highly-developed morphology, not fixed stoichiometry, and mixed crystalline phases [11].

The Pourbaix diagram predicts copper passivity in neutral and alkaline solutions [16]. However, electrooxidation of copper is usually performed in highly alkaline solutions of NaOH [17] or KOH [18] in a three-electrode setup using a potentiostat (i.e., passivation). It results in the formation of the insoluble, passive layer of copper oxides (Cu_2O, CuO) and hydroxide ($Cu(OH)_2$) [19]. There is a general agreement that the form of the anodic film generated on copper depends on the applied electrode potential and can be a simple Cu_2O layer or a duplex Cu_2O/-CuO + $Cu(OH)_2$ structure. The passive film containing Cu(II) compounds has a double structure – an inner layer grown via a solid-state mechanism, and an outer layer formed by nucleation and further growth from the solution. Recently, we have studied the passivation of copper in NH_4HCO_3 solutions, leading to the formation of "pom-pom-like" nanowire clusters [20]. Although the method is economically viable due to very low applied potential, it is limited to laboratory-scale synthesis.

Alternatively, electrooxidation can be performed in a two-electrode setup (i.e., anodization) using a less expensive direct current supply and much larger copper samples. As shown, copper anodizing in 3 M KOH leads to the formation of Cu_2O nanograins, CuO nanosheets, and $Cu(OH)_2$ nanorods, depending on the process duration at a constant current of 6 mA [21]. Recently, less alkaline solutions of K_2CO_2 [22], $KHCO_3$ [23], and $NaHCO_3$ [24] were used as electrolytes for copper anodization, leading to the formation of nano- or micro-wires with a diameter of 100 nm – 10 μm. To the best of our knowledge, bicarbonate solutions have never been used as electrolytes for low-voltage, two-electrode anodization of copper.

It is important to note that carbonate and bicarbonate solutions were extensively studied as electrolytes for corrosion studies of copper in the '90s and early '00s using cyclic voltammetry and rotating disk electrode [25–29]. Carbonates are usually present in the water – especially in hard water – and can have an impact on the corrosion protection of copper pipes caused by other anions [26]. It was recognized that bicarbonate ions prevent copper corrosion [30], and the electrochemical response of copper depends on temperature, pH, ionic strength of the electrolyte, and hydrodynamic conditions (i.e., stirring) [25]. Similarly to anodizing in highly alkaline solutions, the passive layer obtained in carbonates is duplex in nature. However, the layer formed in bicarbonate/carbonate solution is composed of the inner Cu_2O layer, and outer $CuO/Cu_2CO_3(OH)_2$ complex layer, which was confirmed by Electrochemical Impedance Spectroscopy [31] and XPS [32] measurements. Unfortunately, due to the low quality of available SEM images recorded at the time, the in-depth analysis of the formed morphology was unattainable [30,33,34].

In the last decade, CO_2RR reduction on copper-based catalysts became one of the most intensively developing fields in material science and catalysis, with hundreds of papers published each year. Oxide-derived copper materials are well-known to support C—C coupling during CO_2 electroreduction resulting in the formation of highly C_{2+} hydrocarbons and oxygenates [35,36]. This ability can be amplified by numerous factors that originate from altering the metal surface by oxidation treatment [37]. Oxidation of copper, e.g., anodization, provides nanostructured morphologies that significantly expand the surface area available for catalysis. Additionally, new and diverse active sites, such as grain boundaries are generated during the process. The exact reason behind the improved selectivity for C_{2+} products of the oxide-derived copper materials is still under debate [38,39]. Some authors claim that this is due to the enriched with sub-surface oxygen and mixed-valance copper sites ($Cu/Cu^+/Cu^{2+}$) present after electroreduction [38]. Recently, other authors suggested that the improved faradaic efficiency of CO_2 toward C_{2+} products is associated with the presence of malachite at the surface of copper [39–41]. According to our knowledge, only Spodaryk et al. [40] used a chemical method for malachite formation to further study this effect. However, the proposed method was highly time-consuming (over 36 h of synthesis). The low-voltage anodization of copper proposed in this manuscript provides an alternate methodology for a much faster and controllable route to the synthesis of malachite-containing material.

From the material engineering point of view, the search for novel electrooxidation regimes of copper, yielding novel morphologies is a significant scientific task. Moreover, a better understanding of correlations between experimental conditions and the obtained morphologies will enable tailoring the formed material for specific applications. Therefore, we had undertaken the necessary work to gain knowledge on the morphology of copper-derived materials formed by low-voltage anodizing of Cu in $NaHCO_3$ solution, which was explored for the first time. The as-prepared materials were characterized in terms of morphology, composition, and crystalline structure, and subsequently used as the electrode for carbon dioxide reduction reaction, in order to demonstrate possible applicability.

2. Materials and methods

Copper foil (Avanti, Poland, 99.99%, 0.5 mm thickness) was cut into 2.5 cm^2 pieces which were washed in acetone (POCH) and ethanol (POCH, 96%), and then electropolished in 10 M H_3PO_4 (POCH, 85%) solution for 2 min. at the applied cell voltage of 10 V. The electropolishing solution was stirred and kept at 20 °C. During electropolishing, the Cu sample was used as an anode and Pt mesh as a cathode. The as-prepared samples were rinsed thoroughly in water and ethanol, and finally air-dried. Each sample was covered with acid-resistant paint to limit the working surface area precisely to 1 cm^2. To remove any native oxide formed during sample storage, the Cu coupons were cleaned for ca. 1 s in HCl (POCH, 38%), and then rinsed thoroughly with ultrapure water directly before each anodizing process.

Anodic oxidation of copper was performed in a stirred (200 RPM) aqueous solution of $NaHCO_3$ (Eurochem) at 20 °C. The electrolyte solution was prepared directly before the experiment using ultrapure water and used only once. Both the applied cell voltage as well as the used electrolyte concentration were studied in a range of 0.5 – 2.5 V and 0.1 – 0.5 M $NaHCO_3$, respectively. The duration of the anodic oxidation was 3 h unless specified differently. The copper sample was used as an anode and the Pt mesh as a cathode. The distance between the electrodes was maintained constant for all performed anodizing experiments. The current density (j) vs. time (t) dependencies were collected using APPA 207 Multimeter connected to the computer. After anodization, each sample was rinsed delicately in ultrapure water to prevent any disturbance of the formed layer and finally air-dried. Each anodization was performed at least 3 times to check the repeatability of the material formation. Photographs of formed samples were captured using RGB camera.

The morphology of formed anodic layers was studied using field emission scanning electron microscopy (FE-SEM, Quanta 3D, FEI) at 10.0 kV, and at a low vacuum.

The phase analysis was performed using the X-ray diffraction (XRD, Rigaku ULTIMA IV diffractometer) and Match software. Our previous research revealed that the Cu substrate exhibits two very strong reflexes at 2θ of 50.8° and 59.4° corresponding to the (111) and (200) planes, respectively. As the intensity of these reflexes would impede the analysis of other peaks, the presented patterns were recorded in a limited 2θ range of 20 – 50°. The data was collected using a CoK_α radiation source, with a step size of 0.02° and an acquisition rate of 1° per minute.

The surface composition of formed materials was studied by performing X-ray photoelectron (XPS) analysis with a PHI-TFA XPS spectrometer (Physical Electronic Inc.) with an X-ray Al-monochromatic source. During the XPS measurement the vacuum was 10^{-9} mbar. The maximum analysis depth was limited to 10 nm, and the analyzed area was ca. 0.13 cm^2. To collect the peaks narrow multiplex scans at a take-off angle of 45° to the sample surface, and a pass energy of 29.35 eV (step size 0.1 eV) was utilized. For surface charge neutralization a low

energy electron gun was used. Multipak v8.0 (Physical Electronics Inc.) software was used for spectra processing. Curve-fitting was performed for high-energy resolution spectra of Cu 2p, O 1s and C 1s.

Additionally, the composition of formed layers was confirmed using Raman Spectroscopy (RS, Multilaser Confocal Renishaw InVia Reflex Raman spectrometer). The measurements were performed using laser with a wavelength of 532 nm. The laser excitation power was ca. 200 μW on the sample. A one-second integration time and 50 accumulations at the point were used. Each collected spectra was an average from at least 10 spots.

The X-ray Absorption Spectroscopy (XAS) measurements were performed at the SOLARIS National Synchrotron Radiation Centre, Jagiellonian University, at the 04 BM PIRX beamline. A bending magnet (1.31 T), providing photon energy from 100 to 2000 eV, is a source in the PIRX beamline [42]. The beamline optics provide energy resolution lower than $2.5 \bullet 10^{-4}$ with moderate focusing (spot size 250 μm horizontal x 40 μm vertical at the sample). The copper $L_{2,3}$-edge spectra were collected at room temperature using total electron yield (TEY) detection mode.

Electrochemical carbon dioxide reduction reaction (CO_2RR) was studied in a custom-made H-type electrochemical cell (redoxme AB, Norrköping, Sweden). The compartments of the cell were separated with a Nafion 117 membrane. The working electrode, i.e., anodized copper, was placed in a cathodic compartment in a 0.1 M $KHCO_3$ solution. A Pt foil was used as a counter electrode and was placed in an anodic compartment, also filled with 0.1 M $KHCO_3$ solution. The Ag|AgCl|sat. KCl reference electrode was placed in a separate compartment. Before CO_2RR experiments the cathodic compartment was saturated with high purity (99.9999%, Air-Products) CO_2 gas, at a flow rate of 45 ml min^{-1} for 30 min, achieving pH of the electrolyte equal to 6.8. The electrochemical surface area (ECSA) was established by double-layer capacitance measurements in a non-faradaic potential range, in a scan rate range of 20 – 100 mV s^{-1}. The current density (jgeo) was calculated using geometric surface area.

3. Results and discussion

The optimization of material synthesis was performed in four stages. Firstly, the influence of the applied cell voltage during electrooxidation on the morphology and crystalline structure of prepared materials was studied using FE-SEM and XRD, respectively. In the second stage, the influence of the electrolyte concentration on the above-mentioned parameters was established, including Raman Spectroscopy to confirm the composition of the formed material. Next, the influence of the applied cell voltage on the obtained morphology and crystalline structure was studied in a selected concentration of the electrolyte. Finally, the development of surface morphology during copper anodization in 0.4 M $NaHCO_3$ solution at 1 V was established. For the samples prepared at optimized conditions of synthesis, an analysis of composition and crystalline structure was performed using XPS and XAS. This type of sample was selected for testing in CO_2RR.

3.1. Copper anodizing in 0.1 M $NaHCO_3$ at the low applied voltage

Previously it was shown that the optimal regime for copper anodization in 0.01 M $NaHCO_3$ was 25 V [24]. However, the measured current densities were very high (over 30 mA cm^{-2}). Moreover, a significant amount of Cu electrode material was consumed, i.e., dissolved in the used electrolyte solution during the process. From the practical point of view, the application of milder conditions, with lower energy requirements and decreased copper consumption, would be much more preferred. Interestingly, the currents used during the passivation of copper in highly alkaline solutions, leading to the formation of nanostructured oxides, were significantly lower, i.e.; 6 mA [21]. In order to obtain similarly low currents during Cu anodizing in sodium bicarbonate solutions, the applied cell voltage has to be lower than 5 V, as it was assessed during the preliminary screening of anodizing conditions. Therefore, in the first stage of this research, the copper anodizing was performed in 0.1 M $NaHCO_3$ solution at the applied cell voltage in a range of (0.5 – 2.5) V for 6 h. The recorded current density (j) vs. time (t) dependencies, as well as photographs of the obtained samples, are presented in Fig. 1.

Both the morphology and the shape of the recorded j vs. t dependencies strongly depend on the applied cell voltage. For all the samples, the mirror-like copper surface was altered significantly by anodizing in these conditions. During anodization at 0.5 V, the Cu sample turned dark, resembling an "oil spill", without a visible change in texture. At the same time, anodic current density dropped from ca. 0.5 mA cm^{-2} at the beginning of the process to 0.04 mA cm^{-2} at the end. This shape of the curve is typically observed during electrochemical passivation. For the sample prepared at 1.0 V, the copper surface became decorated with unevenly and randomly distributed dark spots. Such spots were formed during the initial drop of the current density (from 1.9 mA cm^{-2} to 0.3 mA cm^{-2}) in the first 1500 s of the process. A similar drop was observed for the samples prepared at higher voltage (i.e., 1.5, 2.0 and 2.5 V), however, instead of achieving a plateau, the current density recovered, and significantly increased in the later stage of anodization. Interestingly, the current density vs. time plot was jagged due to the oxygen bubbles evolution for the anodizing voltage higher than 1.5 V. During electrooxidation at this particular voltage value, the surface of copper becomes much rougher and darker. The same morphology, accompanied by bluish-green precipitates, was observed for the sample prepared at 2.0 V. The bluish-green precipitates covered the whole surface of the sample prepared at 2.5 V. Similar precipitates were observed previously by Milosev et al. [26] during copper passivation in 0.1 M $NaHCO_3$ + 0.1 M Na_2SO_4 at 0.305 V vs. SCE. The sharp increase in the current density was observed around 11500 s for the sample anodized at 2.5 V, resulting from partial delamination of this precipitate.

Subsequently, both the morphology and crystalline state of the anodized samples were studied. The FE-SEM images of the anodized copper as well as the corresponding X-ray diffraction patterns are presented in Fig 2a–d, respectively. Importantly, the stability of the powdery precipitates at the surface of the samples obtained during anodization at 2.0 V and 2.5 V was very low, therefore it was not possible to safely employ FE-SEM imaging due to superficial precipitate delamination under vacuum conditions.

In the case of the sample anodized at 0.5 V (Fig.2a), clusters (ca. 3 μm in diameter) of ribbons (ca. 0.4 μm in diameter) were formed at the surface of copper. The presence of singular XRD reflex at 45.80° for all samples was attributed to the not shielded Kβ reflection of the Cu(111) plane. Interestingly, the intensity of this reflex decreased with applied cell voltage, due to the increasing amount of material formed at the copper surface. Any reflection implying the presence of crystalline Cu_2O, CuO, $Cu(OH)_2$ or Cu_4O_3 was not detected here. Therefore, those compounds are either not present or present in the amorphous phase. Considering the shape of the j vs. t curve (Fig. 1) – i.e., a significant decrease of the current density – it can be assumed that at the initial stage of the anodization at 0.5 V the whole surface of copper was covered with an insulating layer, which limits the charge transfer. Additionally, as FE-SEM imaging revealed, the formation of clusters of ribbons occurred at the surface of this layer. The formed clusters insulate the Cu surface, which limits charge transfer, and therefore further progress of copper oxidation is hindered, leading to decreased rate of malachite formation. This, in turn, led to a decrease in the anodic current density value. It is important to point out that prolonged anodization (i.e., 16 h) at this voltage did not lead to further growth of the clusters. The specific macroscopic appearance of the sample could be explained by specific interactions of formed clusters with light.

Similar clusters of micro-ribbons were observed for the sample anodized at 1.0 V. Such clusters were formed inside the nonuniformly distributed corrosion pits which were spread all over the copper surface. Interestingly, both the diameter of clusters, as well as the diameter of

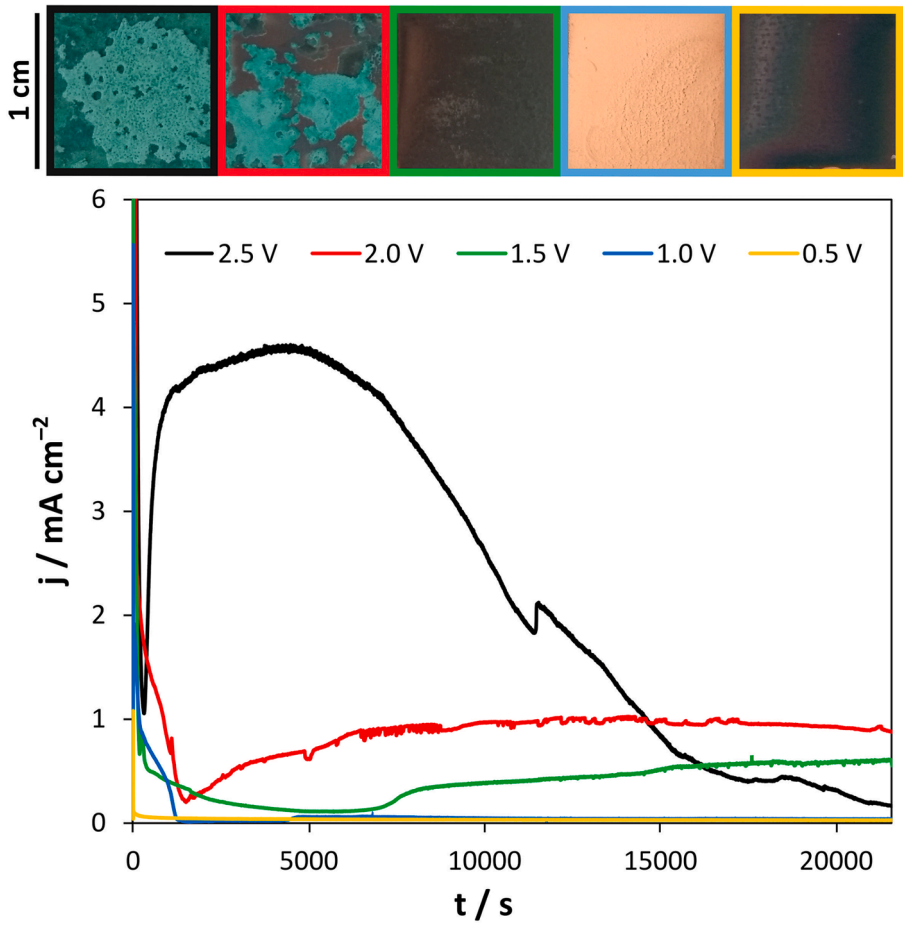

Fig. 1. The photographs of copper samples anodized for 6 h in 0.1 M $NaHCO_3$ at 0.5 – 2.5 V (top) and corresponding current density (j) vs. time (t) plots (bottom).

ribbons were smaller than for the sample prepared at 0.5 V. It can be expected that the rate of oxidation and dissolution of copper inside the corrosion pits is significantly increased, leading to a higher concentration of Cu(II) species in the electrolyte inside those pits. This, in turn, would influence the rate of clusters formation. Anodization at 1.5 V resulted in complete coverage of the Cu surface with the passive layer. According to Kaluzhina and Sieber [32], bicarbonate anions play a protective role in the stabilization of passive film on copper. The observed cracks in this layer are due to the volume expansion, commonly observed during the electrooxidation of some metals, such as aluminum or titanium. The appearance of such cracks could also explain the increased current density after ca. 7000 s, as the insulating layer thickness is locally decreased, exposing the bulk Cu, and increasing charge transfer. Among all samples, only the one prepared at 1.0 V applied cell voltage is promising for further optimization.

Several additional XRD reflections were observed for samples prepared at a cell voltage of 1.0 V and higher. The reflections at 20.50°, 28.16°, 36.52°, 37.62°, and 41.88° correspond to planes (020), (021), (022), (10–2), and (042) of $Cu_2CO_3(OH)_2$, i.e., malachite, respectively. Melendres and Hahn [43] showed that the layer formed by 5 min of potentiostatic passivation of copper at 0.2 V in 0.01 M $NaHCO_3$ consisted mainly of malachite, $Cu(OH)_2$, and possibly some CuO. In order to better understand why the malachite was the main crystalline phase observed here, the previously reported mechanism of Cu passivation in carbonate and bicarbonate mixture should be considered [44,45]. González et al. [44] and Zhou et al. [45] proposed two slightly different sets of consecutive reactions leading to the formation of several possible products during copper passivation in solutions containing $NaHCO_3$ and Na_2CO_3. Both reports are in agreement that at pH range from 9 to 11, layers formed by copper oxidation in presence of bicarbonates are composed of three main constituents: Cu_2O, CuO, and Cu(II)-basic carbonates (malachite/azurite). On the one hand, González et al. [44] showed that the initial stages of the passive layer formation should involve the formation of a thin inner Cu_2O layer followed by the growth of a complex $CuO/Cu_2CO_3(OH)_2$ outer layer. The $Cu(OH)_2$/basic copper carbonates ratio would depend on both pH of the solution and the applied potential. However, they assumed that Cu_2O can be further oxidized to CuO, and malachite/azurite is formed due to nucleation from the electrolyte. On the other hand, Zhou et al. [45] confirmed the formation of CuO—$Cu(OH)_2$ layer at the surface of copper using quartz microbalance, as well as formation of soluble copper species in solution. In fact, they have proven that the malachite/azurite is formed by further electrooxidation of Cu_2O, and CuO is most probably formed by direct oxidation of copper. The most important occurring reactions proposed by Zhou et al. [45] are discussed below.

During electrooxidation of copper at higher potentials CuO can be formed according to (Eq.1) or (Eq.2):

$$Cu + H_2O = CuO + 2H^+ + 2e \quad (1)$$

$$Cu + 2H_2O = CuO{\cdot}H_2O + 2H^+ + 2e \quad (2)$$

Subsequently malachite (Eq.3) or azurite (Eq.4) could be formed due to interactions of Cu_2O and HCO_3^-:

$$Cu_2O + HCO_3^- + H_2O = [Cu_2CO_3(OH)_2] + H^+ + 2e \quad (3)$$

$$3Cu_2O + 4HCO_3^- + H_2O = 2[Cu_3(CO_3)_2(OH)_2] + 2H^+ + 6e \quad (4)$$

The stability constants (logK) of products of the reactions (Eq.3) and (Eq.4) are ca. 34 and 46, respectively [46]. However, Zhou et al. [45] confirmed that malachite is the only observed product.

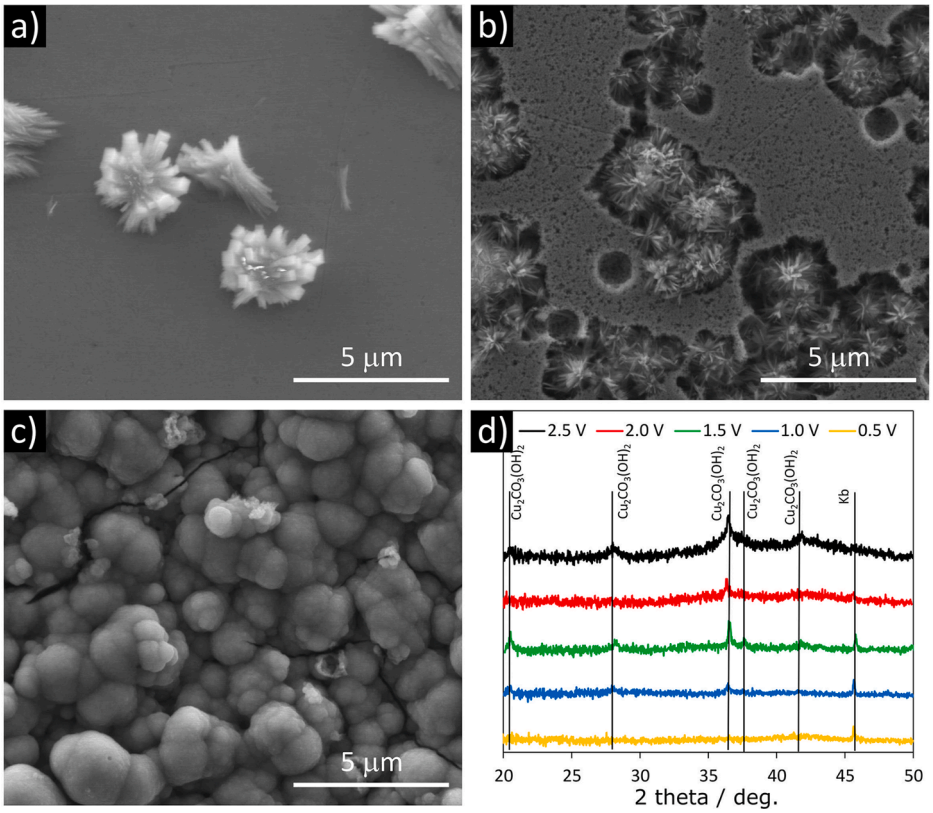

Fig. 2. The FE-SEM images of the copper samples anodized in 0.1 M $NaHCO_3$ at 0.5 V (a), 1.0 V (b) and 1.5 V (c). The respective XRD patterns of copper samples anodized at 0.5 – 2.5 V (d).

At the same time, the formation of Cu_2O is also possible by electrooxidation (Eq.5), and the copper(I) oxide can react with HCO_3^- existing in a solution yielding $CuCO_3$ (Eq.6)

$$2Cu + H_2O = Cu_2O + 2H^+ + 2e \quad (5)$$

$$Cu_2O + 2HCO_3^- = 2CuCO_3 + H_2O + 2e \quad (6)$$

Cu_2CO_3 can be alternatively formed as in reactions (Eq.7) and (Eq.8) through formation of adsorbed on the copper surface $Cu(OH)_{ads}$:

$$Cu + H_2O = Cu(OH)ads + H^+ + e \quad (7)$$

$$Cu(OH)_{ads} + HCO_3^- = CuCO_3 + H_2O + e \quad (8)$$

The $CuCO_3$ (logK = 6.75) would be further dissolved by HCO_3^- in solution to form $[Cu(CO_3)_2]^{2-}$ (logK = 9.92) due to larger stability constants of the product (Eq.9):

$$CuCO_3 + HCO_3^- = [Cu(CO_3)_2]^{2-} + H^+ \quad (9)$$

As a consequence, the diffusion of the soluble species $[Cu(CO_3)_2]^{2-}$ from the electrode to the bulk solution would result in the part of the Cu cathode material unavoidably etched away into the electrolyte.

At even higher potential values, the HCO_3^- anions are attracted to a more positively charged electrode surface, and more soluble substances can be formed, such as $[Cu(CO_3)_2]^{2-}$ and/or $[Cu(CO_3(OH)_2]^{2-}$. The formation of more stable complexes in the presence of HCO_3^- is more probable than further oxidation of Cu_2O into CuO products [45].

Due to the most promising morphology obtained during anodization at 1.0 V, this cell voltage was selected for further tests. Moreover, because of the fact that most of the passive layer growth is expected to occur at the initial stage of electrooxidation, in subsequent measurements, anodizing duration was limited to 3 h.

3.2. Copper anodizing at 1.0 V in selected concentrations of $NaHCO_3$ solutions

The work of Perez-Sanchez et al. [34] revealed that the HCO_3^- concentration significantly influenced the formation of the passive layer during potentiostatic electrooxidation of copper in carbonate and bicarbonate solutions. For example, at high positive potentials and low HCO_3^- concentrations, Cu pitting could be promoted. For this reason, in the second stage of this research, anodizing at concentrations of $NaHCO_3$ higher than 0.1 M was explored. Cu samples were anodized at a constant value of applied voltage equal to 1.0 V in sodium bicarbonate solutions at selected concentrations in a range of 0.1 – 0.5 M. The photographs of the obtained samples as well as the recorded j vs. t dependences are presented in Fig. 3.

The concentration of the used electrolyte had a significant influence on both the macroscopic appearance of the samples as well as the recorded current density vs. time plots. Generally, the higher the concentration of the used electrolyte the higher the measured current density value has been observed, which is consistent with observations made by Drogowska et al. [33] during copper passivation experiments in bicarbonate ions containing electrolyte. Moreover, with increasing electrolyte concentration, the copper samples became deeper black, similar to samples obtained in our previous study on copper passivation in ammonium bicarbonate [20]. Interestingly, for the Cu samples prepared by anodization in 0.4 and 0.5 M sodium bicarbonate, the copper gained a velvet-like finish. Such appearance could be an indicator of promising light-absorption properties.

The current density in the j vs. t plots follows a very similar trend for all samples. After an initial drop of the current density, its value achieves a local maximum, and further plateau. The value of this local maximum depends on the $NaHCO_3$ concentration, however not linearly. Interestingly, for the samples obtained by anodization in 0.4 and 0.5 M sodium bicarbonate solutions, where the velvet finish was observed, the current

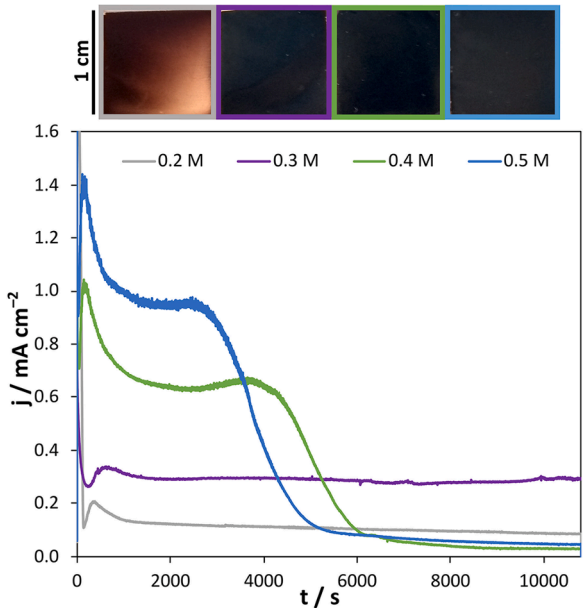

Fig. 3. The photographs of copper samples anodized at 1.0 V applied cell voltage for 3 h in $NaHCO_3$ solutions in the concentration range of 0.1 – 0.5 M (top) and corresponding recorded current density (j) vs. time (t) dependencies (bottom).

density value dropped again, after 3000 s. To correlate the shape of the j vs. t plots with the microscopic morphology of the samples, FE-SEM images were captured and presented in Fig. 4.

Similarly to what was observed for anodization of copper in 0.1 M $NaHCO_3$ at 1.0 V for 6 h (Fig. 2a), during anodization limited to 3 h, the formation of nonuniform pits with ribbon clusters inside them was observed. In their research, Tromans and Sun [47] discussed earlier work on the pitting corrosion of copper. One report stated that the pitting is supposed to be avoided if the pH of the solution is higher than 7 in a solution containing HCO_3^- ions. Such ions are formed due to the hydrolysis/dissociation of $NaHCO_3$ in an aqueous solution. Another report stated that HCO_3^- at a concentration of 0.01 M could promote a pitting corrosion attack on copper in neutral solutions. At higher concentrations (0.1 – 0.5 M) this anion could reduce the protective characteristics of copper-oxide film, mostly due to an increase in soluble copper carbonate complex formation. Conversely, the work of Milosev et al. [26] revealed that an increase in bicarbonate concentration, electrode potential, and exposure time contributes to the formation of a stable layer consisting of precipitated copper oxidation products. Such conflicting reports are not surprising, as copper corrosion and passivation, particularly in bicarbonate solutions, are complex, and influenced by multiple parameters of electrooxidation conditions, as was discussed above.

The surface of the Cu sample formed by anodization in 0.2 M $NaHCO_3$ was nonuniformly etched, with very large corrosion pits merged with each other. Additionally, some individual ribbons were scattered inside these corrosion pits. The surface of copper anodized in 0.3 M sodium bicarbonate solution was covered with clusters of ribbons. Similar morphology was reported for 36 h long chemical synthesis of malachite trees by Spodaryk et al. [40]. However, the shape of the j vs. t plot would indicate that this layer on the copper surface is not completely insulating. The clusters formed at higher electrolyte concentrations (i.e., 0.4 and 0.5 M) were smaller, and individual ribbons could not be easily distinguished. The decrease of the current density after 3000 s for those two samples, could be associated with the moment when the Cu surface became covered with an actual insulating layer composed of copper electrooxidation products. The practical use of the samples prepared by anodization in 0.1 and 0.2 M $NaHCO_3$ at selected conditions is limited, however, the morphology obtained at higher applied cell voltage is more promising.

To gain more information on the possible crystalline and amorphous product of anodization of copper at selected sodium bicarbonate concentrations, the XRD and Raman Spectroscopy experiments were performed, and the results are presented in Fig. 5a and b, respectively.

The XRD results are very consistent with the results presented in Fig. 2. In the case of samples obtained in 0.1, 0.2 and 0.3 M of $NaHCO_3$ only one reflection corresponding to Kβ was observed. For the samples prepared by anodization in 0.1 and 0.2 M $NaHCO_3$ no reflections corresponding to malachite were observed. This is connected with the duration of the anodization. When the anodization was shorter than 6 h, there was not enough time for a significant amount of $Cu_2CO_3(OH)_2$ to be formed. This is consistent with the report of Drogowska et al. [33], which revealed that during prolonged electrooxidation in $NaHCO_3$ solutions, an increased amount of $CuCO_3$ is formed. For the sample prepared at 0.3 M sodium bicarbonate solution, the slight increase of intensity at 2 theta angles corresponding to reflections of malachite was observed, indicating that a small amount of this substance was formed. For the samples anodized in 0.4 and 0.5 M $NaHCO_3$ solutions, the reflections corresponding to malachite are visible, much sharper for the lower concentration. This indicated that the malachite is the only crystalline component of the formed clusters of ribbons.

To confirm the composition of the bulk of the formed material, Raman Spectroscopy was employed. For all the studied samples, several Raman scattering signals of a similar spectral profile were observed. The definite assignment of some peaks proved to be difficult, as they are equivocal across previous reports on copper electrooxidation products [48]. The signals at 152, 220, and 536 cm^{-1} could be attributed to the phonon mode of Cu_2O [49–51]. The wide band observed at values above 600 cm^{-1} can be related to either Cu_2O or CuO [48,51]. The signals at 180 and 589 cm^{-1} could not be unambiguously ascribed. Additional peaks observed in the range of (700–800) cm^{-1} could be the carbonate modes [52,53]. The signals at 304 and 357 cm^{-1} can be associated with the phonon mode of CuO [50], however, the position of the peaks is slightly shifted as compared to the literature reports. The signals at 271, 433, and 474 cm^{-1} compared to phonon mode vibrations observed for $Cu(OH)_2$ are also shifted [48,50]. The peak shift could result from a change in the bonding environment of the Cu(II) centers, perhaps due to coordination with carbonate or bicarbonate, as pointed out by Wang et al. [53]. Because the XRD spectra point out the presence of malachite in the formed material, this effect in the Raman spectra should be also expected. The Raman spectra, reported for malachite, are highly complex, with multiple signals with a similar fingerprint presented in the work here [40].

Based on the results presented in this subsection, it was assessed that the most promising sodium bicarbonate concentration for further exploration is 0.4 M. The passive layer formed in such concentration was the most uniform with a quite unique texture and color. Further optimization of the applied cell voltage in 0.4 M sodium bicarbonate solution was performed.

3.3. *Copper anodizing in 0.4 M $NaHCO_3$ at the low applied voltage*

Copper anodization was performed in 0.4 M $NaHCO_3$ solution at a selected cell voltage range of 0.5 – 2.5 V. The photographs of the prepared samples as well as the recorded j vs. t dependencies are presented in Fig. 6.

Similarly to what was observed for anodizing in 0.1 M sodium bicarbonate solution, the shape of the j vs. t dependencies as well as the appearance of the samples prepared by anodization in 0.4 M $NaHCO_3$ solution strongly depends on the applied cell voltage. The appearance of the samples prepared at 2.0 and 2.5 V is similarly gray, with bluish precipitates present for the latter. The initial shape of the j vs. time dependencies recorded during the anodization of copper at 2.0 and 2.5 V is also very similar. A decrease in the anodic current density in the first

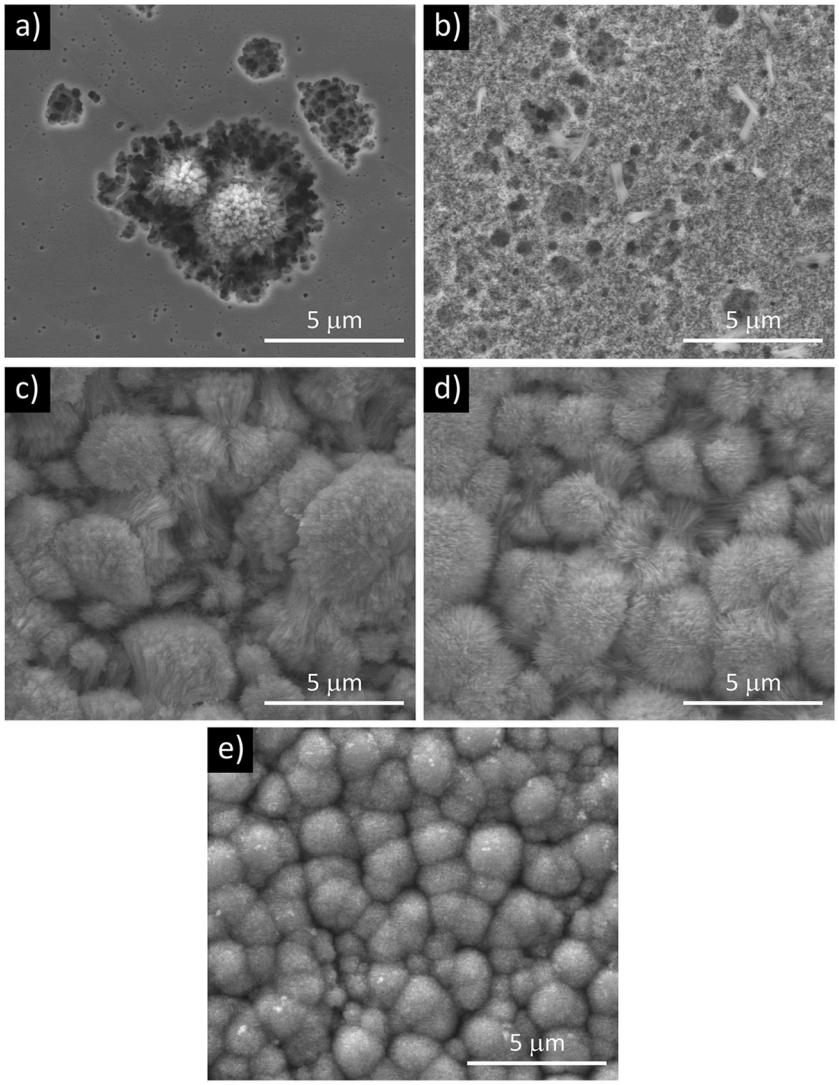

Fig. 4. The FE-SEM images of the copper samples anodized at an applied cell voltage of 1.0 V in $NaHCO_3$ solutions at concentrations of 0.1 (a), 0.2 (b), 0.3 (c), 0.4 (d) and 0.5 M (e).

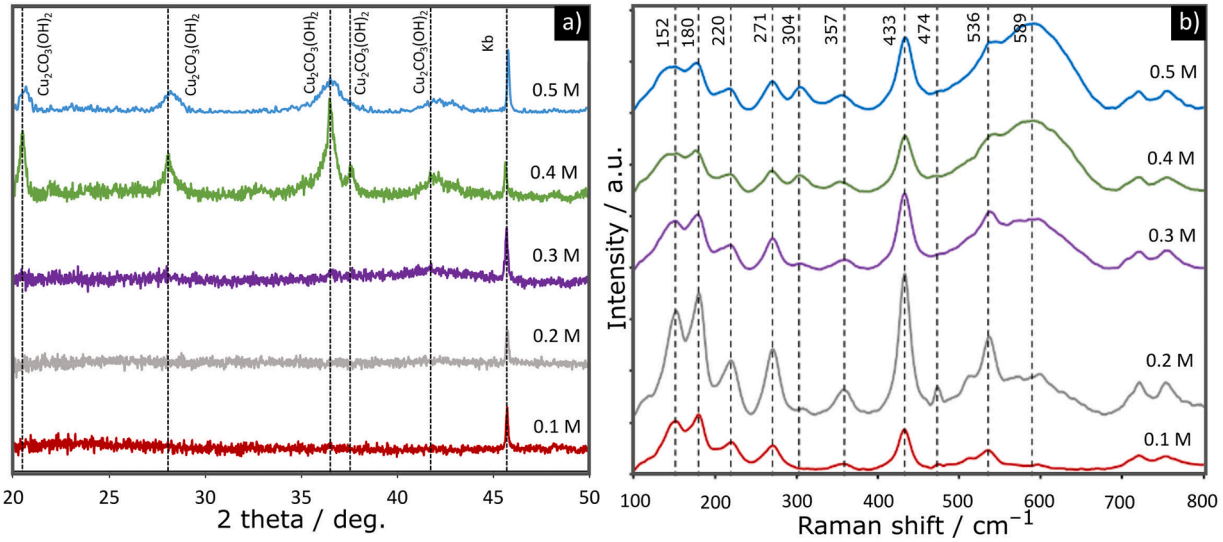

Fig. 5. The XRD patterns of the copper samples anodized at the applied cell voltage of 0.1 V in solutions of $NaHCO_3$ in the concentration range of 0.1 – 0.5 M (a) and the respective Raman spectra (b).

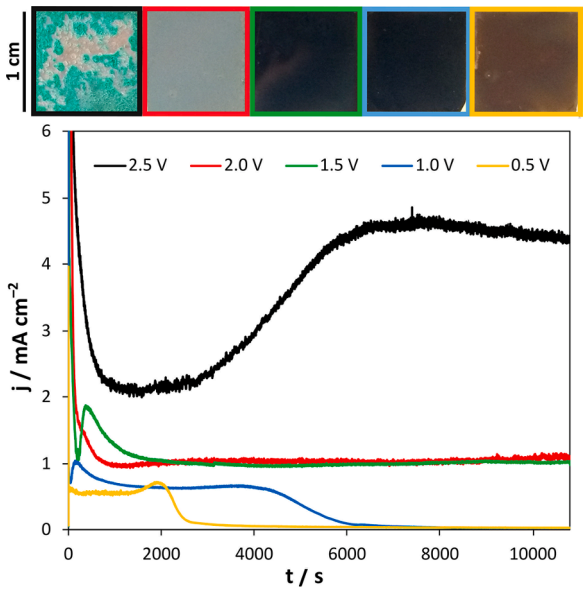

Fig. 6. The photographs of copper samples anodized in 0.4 M $NaHCO_3$ for 3 h at 0.5 – 2.5 V (top) and corresponding current density (j) vs. time (t) plots (bottom).

300 s of anodizing could be related to the increase in the real surface area of the sample due to intensive etching of the Cu leading to increased roughness. However, after 3000 s of anodization increase in the current density was observed, accompanied by the formation of the bluish precipitates. Taking the above-mentioned results into consideration, it could be assumed that this precipitate is malachite.

For the samples prepared at 0.5, 1.0, and 1.5 V, a very similar transient is observed, and the measured current density generally increased with the applied cell voltage. First, a local minimum, and next a local maximum of anodic current density are reached for all of these samples. However, the maximum is achieved in the later stage of anodization for the higher applied cell voltage. Subsequently, a plateau of current density is achieved, which continued to the end of the process at 1.5 V. Conversely, for the samples anodized at 0.5 and 1.0 V, the current density dropped almost to zero. It could be assumed that this decrease in the anodic current density is caused by complete coverage of the copper surface with products of anodization, forming an insulating layer. To confirm such predictions, FE-SEM analysis of as-prepared samples was performed.

In Fig. 7a-d the FE-SEM images are presented for samples prepared by anodization at 1.0 V in selected solutions of sodium bicarbonate for 3 h. The corresponding XRD patterns are presented in Fig. 7e. The stability of the powdery precipitates at the surface of the sample prepared by anodization at 2.5 V was very low, therefore it was not possible to safely employ FE-SEM imagining.

Indeed, the surface of copper is completely covered with clusters for the samples prepared at 0.5 and 1.0 V. However, the clusters are much smaller for the former. Individual clusters of ribbons were also formed at the surface of the copper anodized at 1.5 V. For this sample significant part of the Cu surface was covered with corrosion pits, similarly to the sample prepared by anodization in 0.1 M sodium bicarbonate solution at 0.5 V. Finally, the sample obtained by anodization at 2.0 V in 0.4 M $NaHCO_3$ was completely covered with connected corrosion pits. The XRD patterns confirm such observations, as for the samples, prepared by anodization at 1.5 and 2.0 V only Kβ reflection of Cu was observed. For all other samples, the observed reflections are consistent with malachite, however, the peaks are not sharp, except for the sample prepared at 1.0 V. Due to the most promising morphology, this particular sample was selected for subsequent testing.

To further explore the surface composition and oxidation state of the material formed during anodization of copper in 0.4 M $NaHCO_3$ at the applied voltage of 1.0 V, XPS and XAS measurements were performed. High resolution Cu 2p, O 1s and C 1s peaks and their deconvolution are presented in Fig. 8.

XPS survey of the copper sample anodized in 0.4 M $NaHCO_3$ (Fig. 8a) confirmed the presence of Cu, O and C in the anodic film. In the Fig. 8b-d deconvoluted high resolution XPS spectra of Cu, O, and C are shown, respectively. The fit of Cu 2p XPS spectrum show two doublet signals with main peak at 932.3 eV and 934.6 eV that is attributed to Cu_2O [54] and $Cu_2CO_3(OH)_2$ [55,56] with characteristic split between Cu $2p_{3/2}$ and Cu $2p_{1/2}$ eV spin-orbit components of 19.7 eV. The other peaks represent characteristic satellite peaks for copper compounds [54]. The deconvolution confirms that malachite constitutes the major phase in the material. Malachite is also visible in C 1s deconvoluted spectrum from the peak O = C-$(OH)_2$R at 289.4 eV [55]. The second peak at 284.9 eV represents typical C—C/C—H bonds from organic contaminations (Fig. 8d) [57]. The complementary signals have been found in O 1s spectrum. The three peaks at 530.2, 531.3, and 532.4 eV (Fig. 8c)

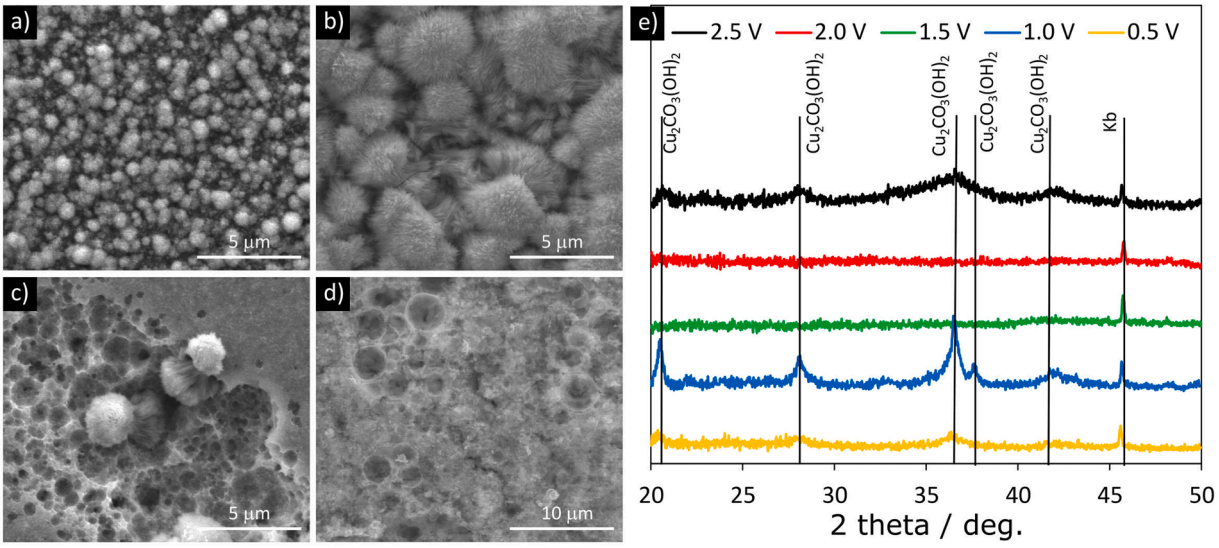

Fig. 7. The FE-SEM images of the copper samples anodized in 0.4 M $NaHCO_3$ at 0.5 V (a), 1.0 V (b), 1.5 V (c), and 2.0 V (d). Respective XRD patterns for samples anodized at 0.5 – 2.5 V.

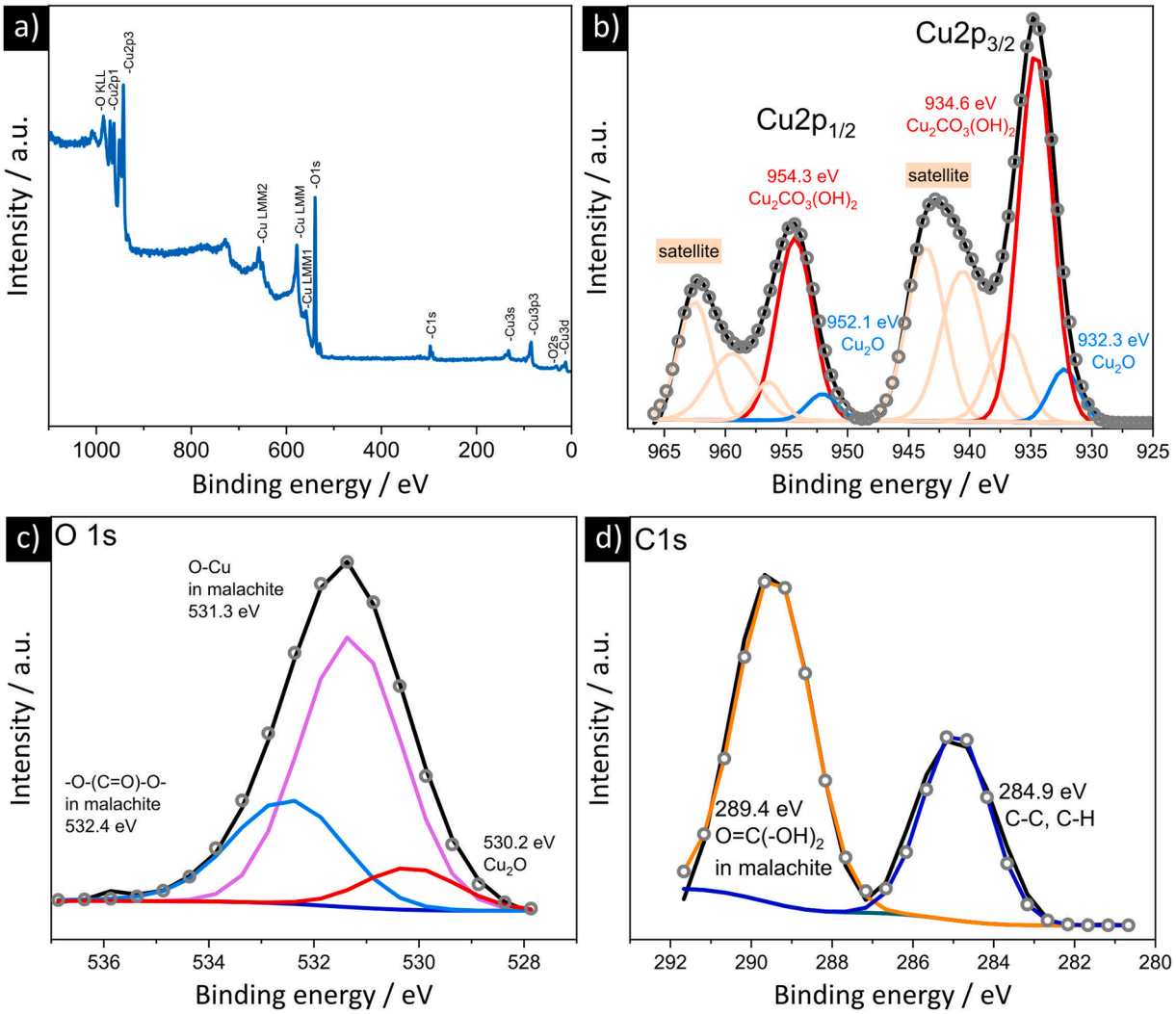

Fig. 8. The XPS survey (a) and high-resolution spectra of Cu 2p (b), O 1 s (c), and C 1 s (d) recorded for the copper sample anodized in 0.4 M $NaHCO_3$ at 1.0 V. .

correspond to Cu_2O [58], Cu-O [55], and -O-(C = O)-O- [59] in malachite, respectively.

To better understand the composition inside the anodic layer, XAS experiments in TEY mode were performed and presented in Fig. 9. This mode provides information about the top several nanometers of the formed material.

The Cu L-edge is presented in Fig. 9a. An intensive peak was observed at 930.9 eV, followed by a small peak at 934.1 eV. An additional peak

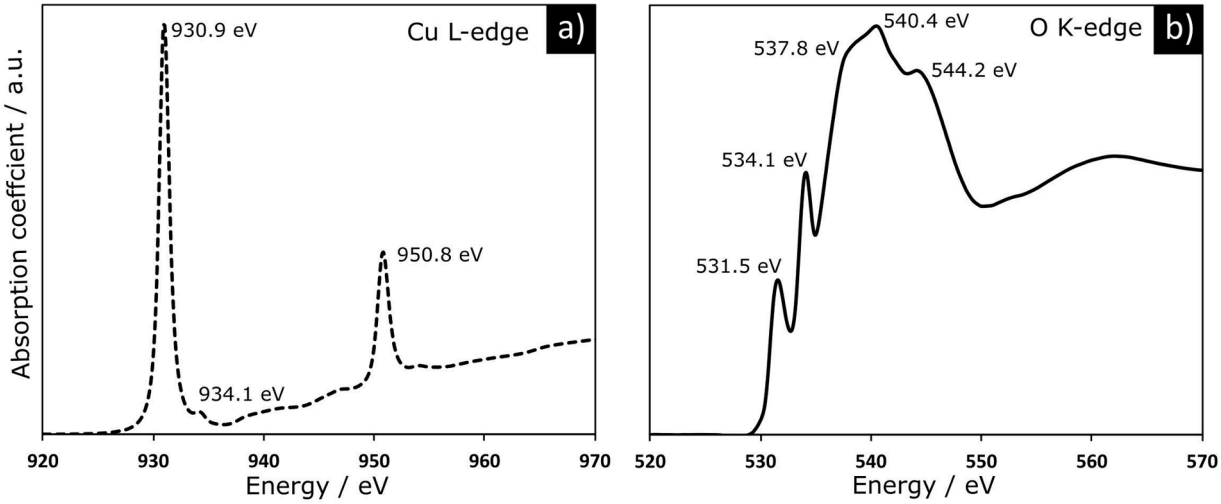

Fig. 9. The XAS Cu L-edge (a) and the O K-edge (b) spectra of copper sample anodized in 0.4 M $NaHCO_3$ at 1.0 V.

was observed at 950.8 eV. The first peak corresponds to the energy of the L3 edge, i.e., excitation from $2p_{3/2}$ to the highest unoccupied 3d state. It is important to note that the energy value of this feature is slightly shifted towards lower energies, as compared to previous reports for CuO [60,61]. Jiang et al. [61] showed that the center energy of this feature could be attributed to the composition of studied Cu(II) compounds, and, consequently, to a different coordination state. Similar energy value of this feature was previously reported for malachite [62] or $Cu(OH)_2$ (i.e., 930.8 eV) [63]. For all those three compounds, the formal copper valence is 2, hence a strong contribution of the Cu d^9 configuration can be expected. The low-intensity peak at 934.1 eV can be attributed to Cu_2O [64]. Finally, the feature at 950.8 eV is related to the L2 transition between Cu $2p_{1/2}$ to unoccupied *d*-states. The energy separation between L2 and L3 features, determined by the spin-orbit coupling is 19.9 eV, which is in good agreement with values reported for CuO and $Cu(OH)_2$, i.e., 19.8 eV [63].

The O K-edge, presented in Fig. 9b is much more complex: two peaks are observed at 531.5 and 534.1 eV, followed by one wide peak with three local maxima at 537.8, 540.4 and 544.2 eV. The first peak is attributed to excitation from 1 s to $3e_g$ [65]. The e_{3g} orbital is formed due to the hybridization of O_{2p} and Cu_{3d} states – partially filled because of the d^9 configuration of Cu(II). Due to a slight shift towards higher energies, as compared with previous reports, this feature could not be ascribed just to CuO [66]. The feature at 534.1 eV could be assigned to 1s - e_g transition typical for Cu_2O. The distance between those two features is consistent with literature reports [65,67]. The broad features observed at the higher energies are assigned to transitions to the hybridized orbitals of oxygen (2p and 3p) and copper (4s and 4p) states.

3.4. Mechanism of passive layer formation during low-voltage anodization

To further explore the mechanism of copper anodizing in 0.4 M $NaHCO_3$ at an applied cell voltage of 1.0 V, the electrooxidation was stopped after different durations during the process. Subsequently, both the macroscopic appearance as well as the microscopic morphology development were studied. The FE-SEM images of anodized copper were correlated with the j vs. t plot and presented in Fig. 10.

The appearance of the copper sample significantly changes during the anodization. Initially, the copper sample becomes darker, however, after 15 min the "oil spill" appearance is gained. After ca. 2 h of anodization, the surface changes color to deep black, with a velvet-like finish. These changes in appearance are correlated with the changes in morphology as well as the shape of the j vs. t plot. The initial current density increase presented in Fig. 10 is connected with the polarization of the electrode. During the first 5 min of anodization, the surface of copper becomes oxidized and the products are dissolved in the electrolyte, leading to slight etching of the copper surface, apparent in the FE-SEM image. Subsequent anodic current density decrease observed in the next 25 min is related to the growth of the clusters on the Cu surface, causing the "oil spill" appearance of the samples. In the next 30 min, the growth of existing clusters as well as the formation of novel ones occurs. Surprisingly, the current density value remains somewhat constant during this stage of copper anodizing. In the next 60 min, as the surface of the copper becomes completely covered with growing ribbon clusters, the current density decreases significantly to 0.03 mA cm^{-2}. Further growth of the clusters is limited, however, the samples gain a bluish hue, assumably due to the increasing amount of malachite, as was discussed earlier.

3.5. Carbon dioxide reduction reaction

The sample with the most promising characteristics (0.4 M $NaHCO_3$; 1 V; 3 h) was selected for further testing in the electrochemical CO_2 reduction reaction (Fig. 11a).

Since the anodized sample chosen for the catalysis tests exhibited morphology of uniformly distributed micro-clusters of even smaller nanostructures it is reasonable to assume significant surface area

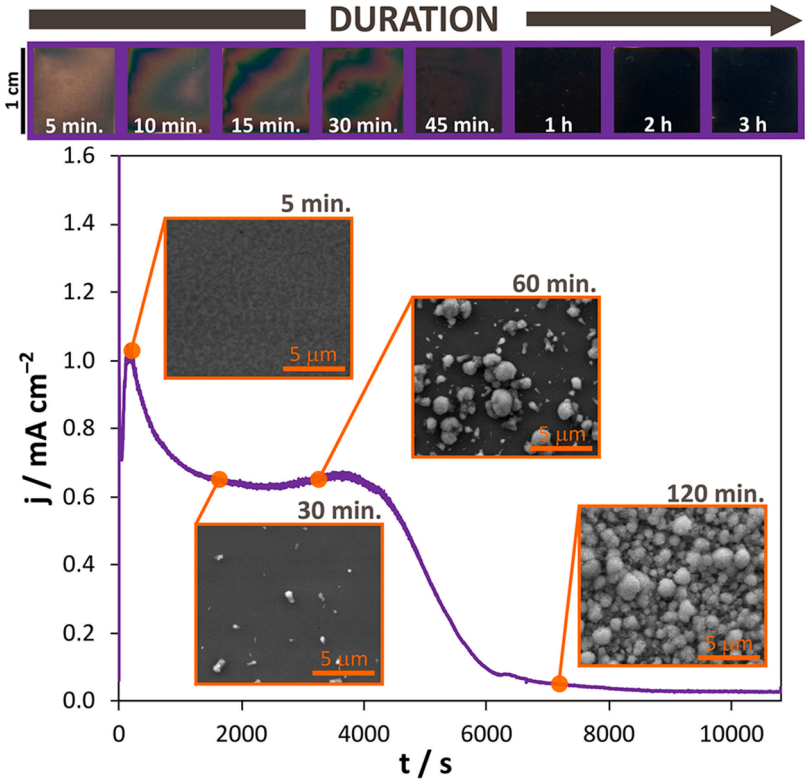

Fig. 10. The photographs of copper samples anodized in 0.4 M $NaHCO_3$ at 1.0 V (top) and corresponding current density (j) vs. time (t) plots (bottom). Insets: The FE-SEM images of the copper anodized for selected durations.

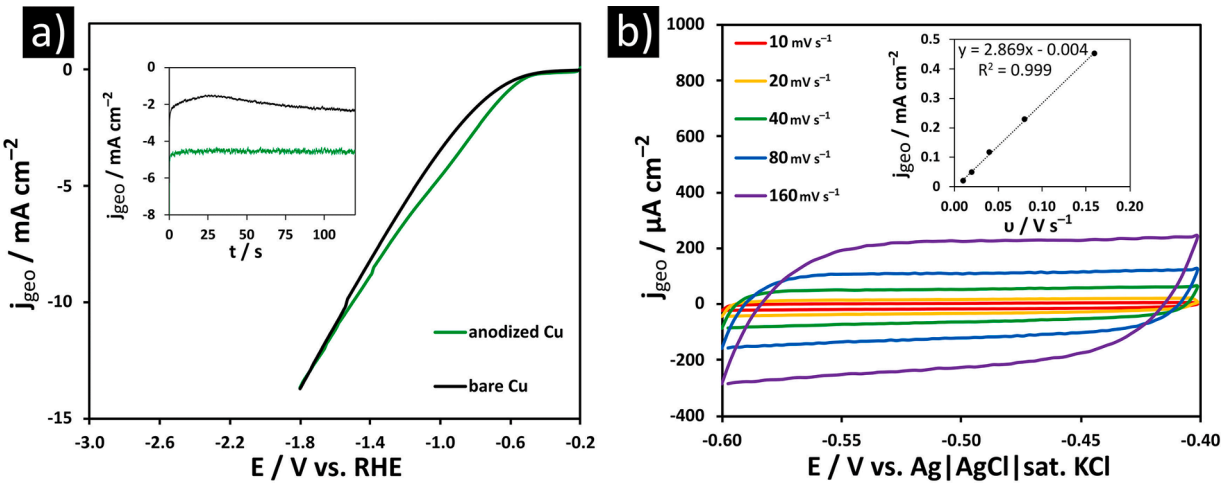

Fig. 11. Linear sweep voltammetry measurement of current density (j_{geo}) vs. potential (E) for anodized Cu and bare Cu working electrodes in 0.1 M $KHCO_3$ (a). Inset: Chronoamperometric measurement for both electrodes measured at potential value −1.05 V vs RHE. ECSA measurement (b). Inset: Current density vs. scan rate plot establishing the capacity of the double layer.

development in the final catalytic material. For that, the sample after chronoamperometric CO_2 reduction was subjected to electrochemical surface area (ECSA) estimation by double layer capacitance (C_{dl}) measurements (Fig. 11b). As it was found, the sample anodized in 0.4 M $NaHCO_3$ at 1 V and after 2 h of CO_2RR indicates C_{dl} of 2.87 mF comparing to 0.02 mF measured for bare copper. Such results show a significant surface development (more than 140 times bigger) achieved by the reported anodization procedure. The electrochemical surface area for the pre-anodized sample exposed to the electrolyte during CO_2RR was found to be 143.5 cm^2.

As presented in Fig. 11a, both linear sweep voltammetry (LSV) and chronoamperometry (ChA) measurements showed improved catalytic properties of the anodized material as compared to bare Cu. LSV voltammogram comparison indicated that applying anodized sample results in a slightly higher cathodic current density in a range of −1.4 V to −0.6 V vs. RHE, thus in the range where there is the highest probability for converting CO_2 into C_{2+} products. To determine the stability of the material in the studied electrocatalytic reaction, the anodized sample was subsequently subjected to chronoamperometric measurements. The potential value of −1.05 V selected for this test was chosen on a basis of recent literature reports on copper-based CO_2RR. It was found that CO_2 is converted into ethylene at this potential in a corresponding catalytic system [68]. As presented, the chronoamperometric curve recorded for the anodized sample indicated superior stability of the material during the whole test. The measured current density after 2 h reached a value of 4.7 mA cm^{-2}. This value exceeds the result obtained for bare copper electrode, i.e.,2.3 mA cm^{-2} after 2 h, showing improvement of the catalytic performance caused by implemented anodization treatment. In the case of the anodized sample, there was no visible change in current density that could be assigned to oxidized copper reduction, consequently implying that the grown anodic layer was reduced at the very initial stage of the CO_2RR experiment. To fully recognize the catalytic potential of the reported material, further optimization is required, especially regarding product selectivity. Nevertheless, these results suggest that low-voltage anodization of copper in bicarbonate-containing electrolyte can be used to synthesize very promising Cu-based electrodes for electrocatalysis.

4. Conclusions

Low-voltage anodization of copper in sodium bicarbonate aqueous solution was studied for the first time. It allowed the formation of material with a developed surface and morphology, which depended both on the applied cell voltage as well as the electrolyte composition. Depending on the applied cell voltage and electrolyte concentration, three general types of morphologies can be obtained – clusters of ribbons, corrosion pits or nonuniform-powdery precipitates. The XAS was applied for the first time for the anodic oxides grown on copper in bicarbonate solutions to help identify the components of the formed layer. The obtained results were in agreement with XPS, XRD, and Raman Spectroscopy results, confirming the presence of Cu_2O and malachite. It can be assumed that low-voltage copper anodizing in sodium bicarbonate solution results in the formation of a mixture of amorphous Cu_2O and crystalline malachite in the clusters of ribbons. Optimization of the experimental conditions (0.4 M $NaHCO_3$, 1 V, 3 h) resulted in the formation of material that was successfully used in the electrochemical carbon dioxide reduction reaction: surface area after anodizing was over 140-times greater than for electropolished copper. It was shown that copper anodizing in sodium bicarbonate solution is an inexpensive, time-efficient, and controllable method to prepare malachite-containing material for greenhouse gas recycling applications.

Author contributions

Conceptualization: A.B.; Data curation: A.B.; Formal analysis: A.B.; Funding acquisition: W.J.S. and D.G.; Investigation: A.B. (material synthesis, FE-SEM, XRD), S.T. (material synthesis), D.G. (CO2RR and XRD), E.W., U.T. and P.T. (XPS), M.L. and B.J. (RS), M. Z. and S.O. (XAS); Projects administration: W.J.S. and D.G.; Supervision: W.J.S.; Visualization: A.B., E.W. and M.L.; Writing – original draft: A.B.

Declaration of Competing Interest

The authors declare that they have no known competing financial interests or personal relationships that could have appeared to influence the work reported in this paper.

Data availability

Data will be made available on request.

Funding

This research was partially funded by the Polish Returns 2019 Project granted by Polish National Agency for Academic Exchange (agreement no. PPN/PPO/2019/1/00003/U/0001) to Wojciech J. Stępniowski. Damian Giziński acknowledges the financial support of the

Polish National Science Centre (NCN-MINIATURA4 DEC- 2020/04/X/ST5/00383) for CO_2RR experiments. Additional support from the statutory research funds of the Department of Functional Materials and Hydrogen Technology, Military University of Technology (grant no UGB 22-788) is appreciated. Safeya A. Taha acknowledges financial support from NAWA PROM Fellowship Program.

References

[1] Ü. Özgür, Y.I. Alivov, C. Liu, A. Teke, M.A. Reshchikov, S. Doğan, V. Avrutin, S.-J. Cho, H. Morkç, A comprehensive review of ZnO materials and devices, J. Appl. Phys. 98 (2005) 1–103, https://doi.org/10.1063/1.1992666.

[2] S. Ida, K. Yamada, M. Matsuka, H. Hagiwara, T. Ishihara, Photoelectrochemical hydrogen production form water using p-type and n-type oxide semiconductor electrodes, Electrochim. Acta 82 (2012) 397–401, https://doi.org/10.1016/j.electacta.2012.03.174.

[3] Y. Zhang, W. Sun, B. Qian, Y. Wang, B. Wang, S. Li, D. Liu, D. Feng, T. Ma, X.-M. Song, Room-temperature photocatalytic methanol fuel cell based on one-dimension semiconductor photoanode: intrinsic mechanism of photogenerated charge separation, Electrochim. Acta 318 (2019) 413–421, https://doi.org/10.1016/j.electacta.2019.06.099.

[4] J.D. Acuña-Bedoya, E. Luévano-Hipólito, E.I. Cedillo-González, L.P. Domínguez-Jaimes, A.M. Hurtado, J.M. Hernández-López, Boosting visible-light photocatalytic degradation of polystyrene nanoplastics with immobilized Cu_xO obtained by anodization, J. Environ. Chem. Eng. 9 (2021), 106208, https://doi.org/10.1016/j.jece.2021.106208.

[5] Y.-H. Zhang, M.-M. Liu, J.-L. Chen, S.-M. Fang, P.-P. Zhou, Recent advances in Cu_2O-based composites for photocatalysis: a review, Dalton Trans. 50 (2021) 4091–4111, https://doi.org/10.1039/d0dt04434b.

[6] B. Liu, C.l. Cai, B. Yang, K. Chen, Y. Long, Q. Wang, S. Wang, G. Chen, H. Li, J. Hu, J. Fu, M. Liu, Intermediate enrichment effect of porous Cu catalyst for CO_2 electroreduction to C_2 fuels, Electrochim. Acta 388 (2021), 138552, https://doi.org/10.1016/j.electacta.2021.138552.

[7] A. Ashok, A. Kumar, F. Tarlochan, Highly efficient nonenzymatic glucose sensors based on CuO nanoparticles, Appl. Surf. Sci. 481 (2019) 712–722, https://doi.org/10.1016/j.apsusc.2019.03.157.

[8] A. Vijayakumar, Y. Zhao, K. Wang, Y. Chao, Z. Chen, C. Wang, G.G. Wallace, The length dependent selectivity on aligned Cu nanowires for C_1 products form CO_2 electroreduction, Electrochim. Acta 394 (2021), 139099, https://doi.org/10.1016/j.electacta.2021.139099.

[9] C. Wang, F. Yang, Y. Cao, X. He, Y. Tang, Y. Li, Cupric oxide nanowires on three-dimensional copper foam for application in click reaction, RSC Adv 7 (2017) 9567–9572, https://doi.org/10.1039/C7RA00014F.

[10] Y. Deng, A.D. Handoko, Y. Du, S. Xi, B.S. Yeo, In situ Raman spectroscopy of copper and copper oxide surfaces during electrochemical oxygen evolution reaction: identification of Cu^{III} oxides as catalytically active species, ACS Catal. 6 (2016) 2473–2481, https://doi.org/10.1021/acscatal.6b00205.

[11] Giziński, D.; Brudzisz, A.; Santos, J.S.; Strixino, F.T.; Stępniowski, W.; Czujko, T. Nanostructured anodic copper oxides as catalysts in electrochemical and photoelectrochemical reactions. Catalysts 2020, 10, 1338. doi:10.3390/catal10111338.

[12] Z. Wang, Y. Zhang, H. Xiong, C. Qin, W. Zhao, .X. Liu, Yucca fern shaped CuO nanowires on Cu foam for remitting capacity fading of Li-ion battery anodes, Sci. Rep. 8 (2018) 6530, https://doi.org/10.1038/s41598-018-24963-2.

[13] S.Y. Lee, H. Jung, N.-K. Kim, H.-S. Oh, B.K. Min, Y.J. Hwang, Mixed copper states in anodized Cu electrocatalyst for stable and selective ethylene production from CO_2 reduction, J. Am. Chem. Soc. 140 (2018) 8681–8689, https://doi.org/10.1021/jacs.8b02173.

[14] S. Anantharaj, H. Sugime, S. Yamaoka, S. Noda, Pushing the limits of rapid anodic growth of CuO/$Cu(OH)_2$ nanoneedles on Cu for the methanol oxidation reaction: anodization pH is the game changer, ACS Appl. Energy Mater. 4 (2021) 899–912, https://doi.org/10.1021/acsaem.0c02822.

[15] M. Mirzaei, A.P. Soleymani, A. Ashrafi, .M..M.. Momeni, Electrochemically enhanced hydrothermal production of cupric oxide photoelectrode on copper substrate, J. Electrochem. Soc. 167 (2020), 066507, https://doi.org/10.1149/1945-7111/ab823b.

[16] M. Pourbaix, Atlas of Electrochemical Equilibria in Aqueous Solutions, 2nd ed., NACE, Houston, TX, 1974.

[17] Y. Wan, Y. Zhang, X. Wang, .W Wang, Electrochemical formation and reduction of copper oxide nanostructures in alkaline media, Electrochem. Commun. 36 (2013) 99102, https://doi.org/10.1016/j.elecom.2013.09.026.

[18] S.D. Giri, A. Sarkar, Electrochemical study of bulk and monolayer copper in alkaline solution, J. Electrochem. Soc. 163 (2016) H252–H259, https://doi.org/10.1149/2.0071605jes.

[19] Y. Ein-Eli, E. Abelev, M. Auinat, D. Starovetsky, Observation of extended copper passivity in carbonate solutions and its future application in copper CMP, Electrochem. Solid-State Lett. 8 (2005) B69–B71, https://doi.org/10.1149/1.2096432.

[20] A. Brudzisz, D. Giziński, E. Wierzbicka, K. Karczewski, U. Tiringer, P. Taheri, W. J. Stępniowski, Pom-pom-like nanowire clusters prepared by potentiostatic oxidation of copper in NH_4HCO_3 solution, Surf. Coat. Technol. 425 (2021), 127674, https://doi.org/10.1016/j.surfcoat.2021.127674.

[21] M. Díaz-Solís, A. Báez-Rodríguez, J. Hernández-Torres, L. García-González, L. Zamora-Peredo, Raman spectroscopy of nanograins, nanosheets and nanorods of copper oxides obtained by anodization technique, MRS Adv. (2019), https://doi.org/10.1557/adv.2019.413.

[22] W.J. Stępniowski, D. Paliwoda, Z. Chen, K. Landskron, W.Z. Misiolek, Hard anodization of copper in potassium carbonate aqueous solution, Mater. Lett. 252 (2019) 182–185, https://doi.org/10.1016/j.matlet.2019.05.126.

[23] W.J. Stępniowski, K.-K. Wang, S. Chandrasekar, D. Paliwoda, A. Nowak-Stępniowska, W.Z. Misiolek, The impact of ethylenediaminetetraacetic acid (EDTA) additive on anodization of copper in $KHCO_3$ – hindering Cu^{2+} re-deposition by EDTA influences morphology and composition of the nanostructures, J. Electroanal. Chem. 871 (2020), 114245, https://doi.org/10.1016/j.jelechem.2020.114245.

[24] D. Giziński, A. Brudzisz, M.R. Alzahrani, K.-K. Wang, W.Z. Misiołek, W. J. Stępniowski, Formation of CuOx nanowires by anodizing in sodium bicarbonate solution, Crystals (2021) 11, https://doi.org/10.3390/cryst11060624.

[25] S.B. Robotta, M.E. Folquer, The effects of temperature and pH on the dissolution and passivation processes of copper in carbonate-bicarbonate solutions, J. Braz. Chem. Soc. 8 (1997) 159–163, https://doi.org/10.1590/S0103-50531997000200013.

[26] I. Milošev, M. Metikoš-Huković, M. Drogowska, H. Ménard, L. Brossard, Breakdown of passive film on copper in bicarbonate solutions containing sulfate ions, J. Electrochem. Soc. 139 (1992) 2409–2418, https://doi.org/10.1149/1.2221241.

[27] B. Beverskog, I. Puigdomenech, Revised Pourbaix diagrams for copper at 25 to 300 °C, J. Electrochem. Soc. 144 (1997) 3476–3483, https://doi.org/10.1149/1.1838036.

[28] M. Drogowska, L. Brossard, H. Menard, Effect of temperature on copper dissolution in $NaHCO_3$ and $NaHCO_3$ + NaCl aqueous solutions at pH 8, J. Electrochem. Soc. 140 (1993) 1247–1251, https://doi.org/10.1149/1.2220965.

[29] S.O. Pehkonen, A. Palit, X. Zhang, Effect of specific water quality parameters on copper corrosion, Corrosion 58 (2002) 156–165, https://doi.org/10.5006/1.3277316.

[30] M. Edwards, T. Meyer, J. Rehring, Effect of selected anions on copper corrosion rates, J. AWWA (1994), https://doi.org/10.1002/j.1551-8833.1994.tb06287.x, 73-18.

[31] M.E. Folquer, S.B. Ribotta, S.G. Real, L.M. Gassa, Study of copper dissolution and passivation processes by electrochemical impedance spectroscopy, Corrosion 58 (2002) 240–247, https://doi.org/10.5006/1.3279875.

[32] S.A. Kaluzhina, I.V. Sieber, Copper passivity and its breakdown in sodium bicarbonate solutions: a scanning electron microscopy and X-ray photoelectron and Auger Spectroscopy study, Russ. J. Electrochem. 42 (2006) 1352–1357, https://doi.org/10.1134/S1023193506120135.

[33] M. Drogowska, L. Brossard, H. Menard, Comparative study of copper behaviour in bicarbonate and phosphate aqueous solutions and effect of chloride ions, J. Appl. Electrochem. 24 (1994) 344–349, https://doi.org/10.1007/BF00242064.

[34] M. Pérez Sénchez, R.M. Souto, M. Barrera, S. González, R.C. Salvarezza, A.J Arvia, A mechanistic approach to the electroformation of anodic layers on copper and their formation in aqueous solution containing NaHCO3, and Na2CO3, Electrochim. Acta 38 (1993) 703–715, https://doi.org/10.1016/0013-4686(93)80242-R.

[35] A. Bagger, W. Ju, A.S. Varela, P. Strasser, J. Rossmeisl, Electrochemical CO_2 reduction: a classification problem, ChemPhysChem 18 (2017) 32660–33327, https://doi.org/10.1002/cphc.201700736.

[36] Y. Hori, K. Kikuchi, A. Murata, S. Suzuki, Production of methane and ethylene in electrochemical reduction of carbon dioxide at copper electrode in aqueous hydrogencarbonate solution, Chem. Lett. 15 (1986) 897–898, https://doi.org/10.1246/cl.1986.897.

[37] F.S. Roberts, K.P. Huhl, A. Nilsson, High selectivity ethylene form carbon dioxide reduction over copper nanocube electrocatalysts, Angew. Chem. 127 (2015) 5268–5271, https://doi.org/10.1002/anie.201412214.

[38] Q. Lei, H. Zhu, K. Song, N. Wei, L. Liu, D. Zhang, J. Yin, X. Dong, K. Yao, N. Wang, X. Li, B. Davaasuren, J. Wang, Y. Han, Investigating the origin of enhanced C_{2+} selectivity in Oxide-/hydroxide-derived copper electrodes during CO_2 electroreduction, J. Am. Chem. Soc. 142 (2020) 4213–4222, https://doi.org/10.1021/jacs.9b11790.

[39] S. Jiang, L. D'Amario, H. Dau, Copper carbonate hydroxide as precursor of interfacial CO in CO_2 electroreduction, ChemSusChem 15 (2022) 1–13, https://doi.org/10.1002/cssc.202102506.

[40] M. Spodaryk, K. Zhao, J. Zhang, E. Oveisi, A. Züttel, The role of malachite nanorods for the electrochemical reduction of CO_2 to C_2 hydrocarbons, Electrochim. Acta 297 (2019) 55–60, https://doi.org/10.1016/j.electacta.2018.11.124.

[41] D.A. Henckel, M.J. Counihan, H.E. Holmes, X. Chen, U.O. Nwabara, S. Verma, J. Rodríguez-López, J.A. Kenis, A.A. Gewirth, Potential dependence of the local pH in CO_2 reduction electrolyzer, ACS Catal. 11 (2021) 255–263, https://doi.org/10.1021/acscatal.0c04297.

[42] M. Zając, T. Giela, K. Freindl, K. Kollbek, J. Korecki, E. Madej, K. Pitala, A. Kozioł-Rachwał, M. Sikora, N. Spiridis, J. Stępień, A. Szkudlarek, M. Ślęzak, T. Ślęzak, D. Wilgocka-Ślęzak, The first experimental results from the 04 BM (PEEM/XAS) beamline at Solaris, Nucl. Instrum. Methods Phys. Res. B 492 (2021) 43–48, https://doi.org/10.1016/j.nimb.2020.12.024.

[43] C.A. Melendres, F. Hahn, Synchrotron infrared microscopy study of film formation and breakdown on copper; CP1214, WIRMS, AIP Conf Proc (2009), https://doi.org/10.1063/1.3326351.

[44] S. González, M. Pérez, M. Barrera, A.R. González Elipe, R.M. Souto, Mechanism of copper passivation in aqueous sodium carbonate-bicarbonate solution derived

from combined X-ray photoelectron spectroscopic and electrochemical data, J. Phys. Chem. B 102 (1998) 5483–5489, https://doi.org/10.1021/jp981069k.
[45] A. Zhou, D. He, N. Xie, Q. Xie, L. Nie, S. Yao, Electrochemical quartz microbalance probing the electro-formed and electr-reduced products on a copper electrode in aqueous solutions containing $NaHCO_3$ and Na_2CO_3, Electrochim. Acta 45 (2000) 3943–3950, https://doi.org/10.1016/S0013-4686(00)00487-4.
[46] P. Duby, The Thermodynamic Properties of Aqueous Inorganic Copper Systems, International Copper Research Association NSRDS, NBS, 1977.
[47] D. Tromans, R. Sun, Anodic behavior of copper in weakly alkaline solutions, J. Electrochem. Soc. 139 (1992) 1945–1951, https://doi.org/10.1149/1.2069527.
[48] Y. Deng, A.D. Handoko, Y. Du, S. Xi, B.S. Yeo, In situ Raman Spectroscopy of copper and copper oxide surfaces during electrochemical oxygen evolution reaction: identification of Cu^{III} oxide as catalytically active species, ACS Catal. 6 (2016) 2473–2481, https://doi.org/10.1021/acscatal.6b00205.
[49] M. Balkanski, M.A. Nusimovici, J. Reydellet, First order Raman spectrum of Cu_2O, Solid State Commun 7 (1969) 815–818, https://doi.org/10.1016/0038-1098(69)90768-6.
[50] D.S. Zimbovskiy, A.I. Gavrilov, B.R. Churagulov, Synthesis of copper oxides films via anodic oxidation of copper foil followed by thermal reduction, IOP Conf. Ser.: Mater. Sci. Eng. 347 (2018), 012010, https://doi.org/10.1088/1757-899X/347/1/012010.
[51] D.P. Oyarzún Jerez, M. López Teijelo, W. Ramos Cervantes, O.E. Linarez Pérez, J. Sánchez, G. Pizarro, G. Acosta, M. Flores, R Arratia-Pérez, Nanostructuring of anodic copper oxides in fluoride-containing ethylene glycol media, J. Electroanal. Chem. 807 (2017) 181–186, https://doi.org/10.1016/j.jelechem.2017.11.047.
[52] R.L. Frost, W.N. Martens, L. Rintoul, E. Mahmutagic, J.T. Kloprogge, Raman spectroscopic study of azurite and malachite at 298 and 77 K, J. Raman Spectrosc. 33 (2002) 252–259, https://doi.org/10.1002/jrs.848.
[53] L. Wang, K. Gupta, J.B.M. Goodall, J.A. Darr, K.B. Holt, In situ spectroscopic monitoring of CO_2 reduction at copper oxide electrode, Faraday Discuss 197 (2017) 517, https://doi.org/10.1039/c6fd00183a.
[54] M.C. Biesinger, Advanced analysis of copper X-ray photoelectron spectra, Surf. Interface Anal. 49 (2017) 1325–1334, https://doi.org/10.1002/sia.6239.
[55] Q. Feng, W. Zhao, S. Wen, Surface modification of malachite with ethanediamine and its effect on sulfidization flotation, Appl. Surf. Sci. 436 (2018) 823–831, https://doi.org/10.1016/j.apsusc.2017.12.113.
[56] H. Xu, D. Dai, S. Li, L. Ge, Y. Gao, In situ synthesis of novel $Cu_2CO_3(OH)_2$ decorated 2D TiO_2 nanosheets with efficient photocatalytic H_2 evolution activity, Dalton Trans 47 (2018) 348–356, https://doi.org/10.1039/C7DT04096B.
[57] Chen, X.; Wang, X.; Fang, D. A review on C1s XPS-spectra for some kinds of carbon materials. Fuller. Nanotub. Carbon Nanostructures 2020, 1048–105. doi:10.1080/1536383X.2020.1794851.
[58] D.A. Svintsitskiy, A.I. Stadnichenko, D.V. Demidov, S.V. Koscheev, A.I. Boronin, Investigation of oxygen states and reactivities on a nanostructured cupric oxide surface, Appl. Surf. Sci. 257 (2011) 8542–8549, https://doi.org/10.1016/j.apsusc.2011.05.012.
[59] G. Beamson, D. Briggs, High Resolution XPS of Organic Polymers - The Scienta ESCA300 Database, Wiley Interscience, 1992. Appendices 3.1 and 3.2.
[60] W. Xu, X.-.L. Zhang, Z.-.Y. Guo, C. Si, Y.-.D. Zhao, A. Marcelli, D.-.L. Chen, Z.-.Y. Wu, Copper L-edge spectra: multiplet vs. multiple scattering theory, J. Phys. 430 (2013), 012010, https://doi.org/10.1088/1742-6596/430/1/012010.
[61] P. Jiang, D. Prendergast, F. Borondics, S. Porsgaard, L. Giovanetti, E. Pach, J. Newberg, H. Bluhm, F. Besenbacher, M. Salmeron, Experimental and theoretical investigation of the electronic structure of Cu_2O and CuO thin films on Cu(110) using x-ray photoelectron and absorption spectroscopy, J. Chem. Phys. 138 (2013), 024704, https://doi.org/10.1063/1.4773583.
[62] M. Grioni, J.B. Goedkoop, R. Schoorl, F.M. de Groot, J.C. Fuggle, F. Schafers, E. E. Koch, G.I. Rossi, J.-.M. Esteva, R.C. Karnatak, Studies of copper valence states with Cu L3 x-ray-absorption spectroscopy, Phys. Rev. B 39 (1989) 1541, https://doi.org/10.1103/PhysRevB.39.1541.
[63] K. Shimizu, H. Maeshima, H. Yoshida, A. Satsuma, T. Hattori, Ligand field effect on the chemical shift in XANES spectra of Cu(II) compounds, Phys. Chem. Chem. Phys. 3 (2001) 862–866, https://doi.org/10.1039/b007276l.
[64] M. Grioni, J.F. van Acker, J.C. Czyżyk Fuggle, Unoccupied electronic structure and core-hole effects in the x-ray-absorption spectra of Cu_2O, Phys. Rev. B 45 (1992) 3309, https://doi.org/10.1103/PhysRevB.45.3309.
[65] A.B. Gurevich, B.E. Bent, A.V. Teplyakov, J.G. Chen, A NEXAFS investigation of the formation and decomposition of CuO and Cu_2O thin films on Cu (100), Surf. Sci. 442 (1999) L971–L979, https://doi.org/10.1016/S0039-6028(99)00913-9.
[66] F.M.F. De Groot, M. Grioni, J.C. Fuggle, J. Ghijsen, G.A. Sawatzky, H. Petersen, Oxygen 1 s x-ray-absorption edges of transition-metal oxides, Phys. Rev. B 40 (1989) 5715, https://doi.org/10.1103/PhysRevB.40.5715.
[67] S. Saikova, S. Vorobyev, M. Likhatski, A. Romanchenko, S. Erenburg, S. Trubina, Y. Mikhlin, X-ray photoelectron, Cu L3MM Auger and X-ray absorption spectroscopic studies of Cu nanoparticles produced in aqueous solutions: the effect of simple preparation techniques, Appl. Surf. Sci. 258 (2012) 8214–8221, https://doi.org/10.1016/j.apsusc.2012.05.024.
[68] W. Liu, P. Zhai, A. Li, B. Wie, K. Si, Y. Wei, X. Wang, G. Zhu, Q. Chen, X. Gu, R. Zhang, W. Zhou, Y. Gong, Electrochemical CO_2 reduction to ethylene by ultrathin CuO nanoplate arrays, Nature Comm 13 (2022) 1877, https://doi.org/10.1038/s41467-022-29428-9.